Takeharu Iwakiri, Hiromitsu Terao, Enno Lork, Thorsten M. Gesing and Hideta Ishihara*

X-ray and NQR studies of bromoindate(III) complexes: $[C_2H_5NH_3]_4InBr_7$, $[C(NH_2)_3]_3InBr_6$, and $[H_3NCH_2C(CH_3)_2CH_2NH_3]InBr_5$

DOI 10.1515/znb-2016-0207
Received September 19, 2016; accepted October 19, 2016

Abstract: The crystal structures of $[C_2H_5NH_3]_4InBr_7$(**1**), $[C(NH_2)_3]_3InBr_6$(**2**), and $[H_3NCH_2C(CH_3)_2CH_2NH_3]InBr_5$(**3**) were determined at 100(2) K: monoclinic, $P2_1/n$, $a=1061.94(3)$, $b=1186.40(4)$, $c=2007.88(7)$ pm, $\beta=104.575(1)°$, $Z=4$ for **1**; monoclinic, $C2/c$, $a=3128.81(12)$, $b=878.42(3)$, $c=2816.50(10)$ pm, $\beta=92.1320(10)°$, $Z=16$ for **2**; orthorhombic, $P2_12_12_1$, $a=1250.33(5)$, $b=1391.46(6)$, $c=2503.22(9)$ pm, $Z=4$ for **3**. The structure of **1** contains an isolated octahedral $[InBr_6]^{3-}$ ion and a Br^- ion. The structure of **2** contains three different isolated octahedral $[InBr_6]^{3-}$ ions. The structure of **3** has a corner-shared double-octahedral $[In_2Br_{11}]^{5-}$ ion and an isolated tetrahedral $[InBr_4]^-$ ion. The ^{81}Br nuclear quadrupole resonance (NQR) lines of the terminal Br atoms of the compounds are widely spread in frequency, and some of them show unusual positive temperature dependence. These observations manifest the N–H···Br–In hydrogen bond networks developed between the cations and anions to stabilize the crystal structures. The ^{81}Br NQR and differential thermal analysis (DTA) measurements have revealed the occurrence of unique phase transitions in **1** and **3**. When the bond angles were estimated from the electric field gradient (EFG) directions calculated by the molecular orbital (MO) methods, accurate values were obtained for $[InBr_6]^{3-}$ of **1** and for $[In_2Br_{11}]^{5-}$ and $[InBr_4]^-$ of **3**, except for several exceptions in those for the latter two ions. On the other hand, the calculations of ^{81}Br NQR frequencies have produced up to 1.4 times higher values than the observed ones.

***Corresponding author: Hideta Ishihara,** Faculty of Culture and Education, Saga University, Saga 840-8502, Japan,
e-mail: isiharah@cc.saga-u.ac.jp
Takeharu Iwakiri: Faculty of Culture and Education, Saga University, Saga 840-8502, Japan
Hiromitsu Terao: Faculty of Integrated Arts and Sciences, Tokushima University, Tokushima 770-8502, Japan
Enno Lork and Thorsten M. Gesing: Solid State Chemical Crystallography, Institute of Inorganic Chemistry and Crystallography, and MAPEX Center for Materials and Processes, University Bremen, D-28359 Bremen, Germany

Keywords: bromoindates(III); crystal structures; DTA; MO calculations; NQR; phase transitions.

1 Introduction

The crystal chemistry of In(III) complex compounds is characterized by a variety of coordination types taken by the In(III) atom. Carty and Tuck [1] discussed the coordination number of In(III) compounds from the viewpoint of cation sizes and also related to the preparative conditions. We have become interested in the structures of bromoindate(III) complexes with a series of organic ammonium cations. Various structural types of anions with different coordination are expected in their structures depending not only on the cation sizes and charges but also on the hydrogen bonds of N–H···Br–In formed by the cations. We already reported the crystal structures of the complexes with dimethylammonium and 4-chloroanilinium counter ions, that is, $[(CH_3)_2NH_2]_3InBr_6$ and $[4\text{-}ClC_5H_4NH]_2InBr_5$, respectively [2]. It was found that two kinds of isolated octahedral $[InBr_6]^{3-}$ ions exist in the former structure, whereas an isolated distorted square pyramidal $[InBr_5]^{2-}$ ion exists in the latter one. The penta-coordinated complex ion is rarely found in In(III) compounds [1]. The coordination geometry of the bromoindate(III) ions in these crystal structures seems to be very dependent on the cations. For a further investigation we prepared the complexes with three different cations, ethylammonium, guanidinium, and 2,2-dimethyl-1,3-propanediammonium: $[C_2H_5NH_3]_4InBr_7$ (**1**), $[C(NH_2)_3]_3InBr_6$ (**2**), and $[H_3NCH_2C(CH_3)_2CH_2NH_3]InBr_5$ (**3**), respectively. In this article we report the results of ^{81}Br nuclear quadrupole resonance (NQR) and differential thermal analysis (DTA) measurements as well as the crystal structures of the complexes. The molecular orbital (MO) calculations are also applied for the estimation of electric field gradients (EFGs) at the Br nuclei of the bromoindate anions of **1** and **3**. The ^{81}Br NQR frequencies and bond angles calculated from EFGs are compared with the measured values in order to confirm the effectivity of the calculations.

2 Results and discussion

2.1 Crystal structure determination of tetrakis(ethylammonium) heptabromoindate(III) $[C_2H_5NH_3]_4InBr_7$ (1)

A freshly prepared needle crystal (**1N**) was picked for the crystal structure determination, because the crystals turned gradually into massive ones on keeping them in the mother liquor. The crystal structure data obtained at 100 K are listed in Table 1. As described in the next section, it was found that the crystal of **1N** underwent a phase transition. Thus, this structure corresponds to that of the low-temperature phase (LTP), $\mathbf{1N}_{LTP}$. The projection of a unit cell down the *a* axis is shown in Fig. 1. The asymmetric unit is composed of one octahedral $[InBr_6]^{3-}$ ion, one Br^- ion, and four $C_2H_5NH_3^+$ ions. This structure is similar to those of $[CH_3NH_3]_4InBr_7$ ($P2_1/c$, $a=1683.8(6)$, $b=772.2(2)$, $c=2086.4(6)$ pm, $\beta=128.67(2)°$, $Z=4$) [3] and $[CH_3NH_3]_4InCl_7$ ($P2/c$, $a=1611.3(3)$, $b=746.6(5)$, $c=2030.0(8)$ pm, $\beta=127.9(4)°$, $Z=4$) [4], though their asymmetric unit contains two octahedral $[InBr_6]^{3-}$ or $[InCl_6]^{3-}$ ions, but one in $\mathbf{1N}_{LTP}$. The In–Br bond lengths vary from 262.27(4) to 273.98(4) pm in $\mathbf{1N}_{LTP}$, as listed in Table 2, whereas variations from 266 to 268 pm are found in $[CH_3NH_3]_4InBr_7$ [3]. The bond angles ∠Br–In–Br (*cis*) range from 86.60(1) to 93.95(2)° in $\mathbf{1N}_{LTP}$, as shown in Table 3. The corresponding angles in $[CH_3NH_3]_4InBr_7$ [3] change from 89.6 to 90.2°. The slightly larger deviations from the regular octahedron for the $[InBr_6]^{3-}$ ion in $\mathbf{1N}_{LTP}$ than in $[CH_3NH_3]_4InBr_7$ arise from the differences in both shapes of cations and hydrogen bond schema around anions. The hydrogen bonds in $\mathbf{1N}_{LTP}$ are depicted in Fig. 2 and their parameters are listed in Table 4.

2.2 NQR and DTA measurements of $[C_2H_5NH_3]_4InBr_7$ (1); its self-decomposition to $[C_2H_5NH_3]_3InBr_6 + [C_2H_5NH_3]Br$

The temperature-dependence curves of ^{81}Br NQR frequencies of **1N** measured in the range from 77 to around

Table 1: Crystal structure data for **1–3**.

	1	2	3
Formula	$C_8H_{32}N_4Br_7In$	$C_3H_{18}N_9Br_6In$	$C_{15}H_{48}N_6Br_{15}In_3$
M_r	858.52	774.54	1855.70
Cryst. size, mm³	0.376×0.348×0.345	0.25×0.20×0.14	0.2×0.1×0.1
Crystal system	Monoclinic	Monoclinic	Orthorhombic
Space group	$P2_1/n$	$C2/c$	$P2_12_12_1$
Temperature, K	100(2)	100(2)	100(2)
a, pm	1061.94(3)	3128.81(12)	1250.33(5)
b, pm	1186.40(4)	878.42(3)	1391.46(6)
c, pm	2007.88(7)	2816.50(10)	2503.22(9)
β, deg	104.575(1)	92.1320(10)	90
V, Å³	2448.29(14)	7735.5(5)	4355.1(3)
Z	4	16	4
D_{calcd}, g cm^{-3}	2.24	2.66	2.83
μ(MoK_α), mm^{-1}	0.1	0.1	0.2
F(000), *e*	1471	5728	3408
hkl range	$-15 \le h \le +11$	$-40 \le h \le +40$	$-16 \le h \le +16$
	$0 \le k \le +16$	$-11 \le k \le +11$	$-18 \le k \le +18$
	$-11 \le l \le +28$	$-36 \le l \le +36$	$-32 \le l \le +32$
$((\sin\theta)/\lambda)_{max} \times 10^3$, pm^{-1}	7.1665	6.4966	6.4962
Refl. measured	68 798	185 281	34 901
Refl. unique	7531	8884	10 007
R_{int}	0.0592	0.0652	0.0485
Refl. with $I > 2\sigma(I)$	6602	7549	9354
Param. ref./restraints	180/0	346/0	405/36
$R(F)/wR(F^2)$ ($I > 2\sigma(I)$)	0.0318/0.0772	0.0169/0.0359	0.0295/0.0662
$R(F)/wR(F^2)$ (all refl.)	0.0388/0.0844	0.0241/0.0377	0.0336/0.0679
x(Flack)	–	–	[a]
GoF (F^2)	0.5764	1.087	1.046
$\Delta\rho_{fin}$ (max/min) × 10^{-6} *e* pm^{-3}	1.91/–1.04	1.00/–0.56	1.57/–0.95

[a]Refined as racemic twin which disables the Flack parameter. Twin individual mass fractions are 0.497(8) and 0.503(8).

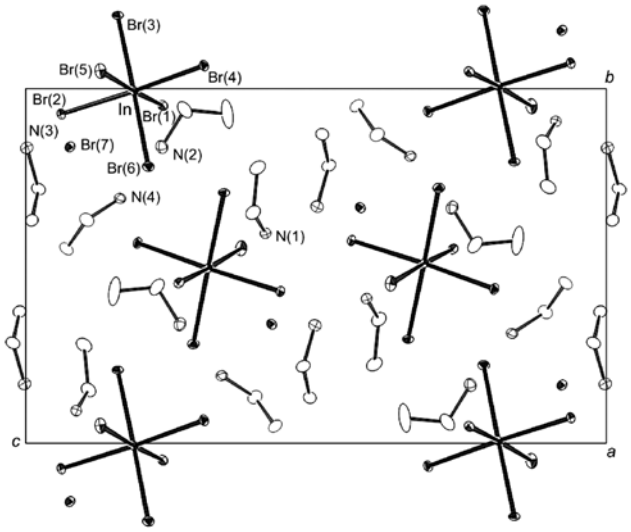

Fig. 1: Projection of the crystal structure of $\mathbf{1N}_{LTP}$ at 100 K down the crystallographic *a* axis.

Table 2: Selected bond lengths (pm) in the bromoindate anions of $\mathbf{1N}_{LTP}$, **2**, and **3** with estimated standard deviations in parentheses.[a]

$\mathbf{1N}_{LTP}$		**2**		**3**	
In–Br1	267.39(4)	In1–Br1	266.93(3)	In1–Br1	270.36(9)
In–Br2	268.21(4)	In1–Br2	263.41(3)	In1–Br2	260.56(10)
In–Br3	273.98(4)	In1–Br3	266.57(3)	In1–Br3	264.32(10)
In–Br4	262.27(4)	In1–Br4	266.44(3)	In1–Br4	262.01(9)
In–Br5	263.86(4)	In1–Br5	270.40(3)	In1–Br5	268.45(9)
In–Br6	268.34(5)	In1–Br6	268.66(3)	In1–Br6	279.82(9)
		In2–Br7	267.24(3)	In2–Br6	301.66(9)
		In2–Br7$^{\#1}$	267.23(3)	In2–Br7	260.05(10)
		In2–Br8	265.15(3)	In2–Br8	264.64(9)
		In2–Br8$^{\#1}$	265.16(3)	In2–Br9	261.76(10)
		In2–Br9	269.78(3)	In2–Br10	267.26(10)
		In2–Br9$^{\#1}$	269.77(3)	In2–Br11	262.57(9)
		In3–Br10	267.68(2)	In3–Br12	256.34(10)
		In3–Br10$^{\#2}$	267.68(2)	In3–Br13	250.50(10)
		In3–Br11	272.38(3)	In3–Br14	250.20(10)
		In3–Br11$^{\#2}$	272.39(3)	In3–Br15	252.16(10)
		In3–Br12	261.86(2)		
		In3–Br12$^{\#2}$	261.87(2)		

[a]Symmetry operations: $^{\#1}$ 1 – *x*, *y*, 1/2 – *z*; $^{\#2}$ 1 – *x*, 1 – *y*, 1 – *z*.

300 K are shown in Fig. 3. In accordance with the crystal structure at 100 K, six ^{81}Br NQR lines showing the same intensities were observed. These lines are assigned to the nonequivalent Br atoms of $[InBr_6]^{3-}$, because the Br^- line should have, if observed, a far lower frequency, less than a few MHz. As seen in Fig. 3, the disappearance of the resonance lines was found between around 110 and 200 K for the highest- and lowest-frequency lines and between around 125 and 160 K for the remaining lines. The disappearance phenomenon may be due to a phase transition as detected by DTA measurements described below. The respective curves of the outer two lines connect smoothly between the low- and high-temperature parts on extrapolation. However, the close existence of the inner resonance lines makes not only the continuity of the curves but also the number of resonance lines themselves ambiguous in the higher temperature region. On the other hand, the NQR spectrum is outstanding for its widespread frequencies spanning to almost 32 MHz at 77 K despite the discrete anion. Furthermore, the ν versus T curve of the lowest-frequency line has an unusually large positive coefficient, though the line has normally a negative value due to the thermal lattice vibrations. The observation may be caused by a dynamical event of the intermolecular interaction related to the Br atoms of $[InBr_6]^{3-}$. In many cases the intermolecular bonds lead to lower frequencies of the relevant lines compared with those of atoms free from such bonds. Then, when the intermolecular bonds are subjected to weakening at increasing temperatures, the positive temperature dependence is seen as a result. It seems that all Br atoms of the $[InBr_6]^{3-}$ ion are more or less involved in the hydrogen bonds with short contacts of N···Br, as listed in Table 4. Among them, the Br3 atoms have the shortest contact with 337.6(3) pm and the longest In–Br bond length with 273.98(4) pm, which indicates the formation of the strongest hydrogen bond. By considering this situation the Br3 atom seems to be the most probable candidate assignable to the lowest NQR frequency line. If this is the case, the *trans*-effect may allow us the further assignment of the highest line to the Br6 atom situated in a *trans*-position of the Br3 atom. This effect predicts that the average NQR frequency of the atoms situated in a *trans*-position of the octahedral complex is kept nearly constant and the corresponding resonance lines, thus, changing their frequencies symmetrically for the counterpart with temperature. This is the consequence of the fact that the bonding in the octahedral complex is well explained using the 3c-4e bond model.

In the course of the NQR measurements, we found that the aged samples $\mathbf{1O}_{(10Y)}$ and $\mathbf{1O}_{(2Y)}$, kept at ambient temperatures for about 10 and 2 years, respectively, produced other extra NQR lines in addition to those of **1N**, as shown in Fig. 4. The DTA measurements for the fresh sample of **1N** showed an exothermic peak at 182 K on the cooling run, whereas the endothermic peaks appeared at 208 and 300 K on the heating run, as depicted in Fig. 5a. The lower-temperature phase transition at 182 K in the cooling run and 208 K in the heating run is a first-order type accompanied with a large hysteresis. The higher-temperature phase transition at 300 K is a second-order type by judging from

Table 3: Bond angles (deg) in the bromoindate anions of $\mathbf{1N}_{LTP}$ and **3** derived from X-ray data structure refinements (upper) and MO calculations (lower).

$[InBr_6]^{3-}$ in $\mathbf{1N}_{LTP}$	Br1	Br2	Br3	Br4	Br5
Br2	89.224(13)				
	89.43				
Br3	86.598(13)	89.165(13)			
	86.10	89.30			
Br4	90.554(14)	177.529(16)	88.365(14)		
	90.35	176.67	88.36		
Br5	173.942(17)	88.231(14)	87.869(15)	91.752(14)	
	172.78	87.72	87.23	92.11	
Br6	91.512(14)	89.215(14)	177.527(15)	93.251(14)	93.949(16)
	91.85	88.91	177.30	94.42	94.71
$[InBr_4]^-$ in **3**	**Br12**	**Br13**	**Br14**		
Br13	105.44(3)				
	104.05				
Br14	100.20(3)	132.00(4)			
	96.30	140.37			
Br15	103.92(3)	104.63(3)	107.62(3)		
	102.36	102.18	106.53		
$[In_2Br_{11}]^{5-}$ in **3**	**Br1**	**Br2**	**Br3**	**Br4**	**Br5**
Br2	93.03(3)				
	94.38				
Br3	91.26(3)	90.16(4)			
	92.33	90.36			
Br4	94.71(3)	172.19(3)	88.65(3)		
	96.89	168.77	87.89		
Br5	92.63(3)	88.10(3)	175.81(4)	92.57(3)	
	94.37	87.20	172.78	94.47	
Br6	178.80(3)	87.94(3)	88.03(3)	84.30(3)	88.09(3)
	173.18	81.99	82.13	86.87	89.01
$[In_2Br_{11}]^{5-}$ in **3**	**Br6**	**Br7**	**Br8**	**Br9**	**Br10**
Br7	84.10(3)				
	74.12				
Br8	87.35(3)	92.92(3)			
	80.04	93.76			
Br9	83.62(3)	167.62(3)	88.09(3)		
	86.88	166.67	87.60		
Br10	79.03(3)	88.33(3)	166.13(4)	87.78(3)	
	86.15	87.28	165.28	88.08	
Br11	172.52(3)	100.11(3)	98.55(3)	91.93(3)	94.83(3)
	176.19	102.22	99.31	90.60	94.80

the peak shape. This phase transition should be accompanied by only a slight structural change, as the corresponding anomaly was not found in the cooling run and also no anomalous changes occurred on the ν versus T curves of ^{81}Br NQR lines in the vicinity of this temperature. The DTA curve of the aged sample of $\mathbf{1O}_{(6M)}$ left for 6 months after preparation is shown in Fig. 5b. On cooling, the exothermic peak split into two peaks without any notable changes in the endothermic peak. Moreover, in the second run after 1 week, no heat anomaly appeared on cooling, but an exothermic peak strangely appeared at 163 K and an endothermic peak shifted to 213 K on heating. On the other hand, the sample $\mathbf{1O}_{(10Y)}$ also exhibited heat anomalies but at different temperatures, at 301 K on the cooling run and at 310 K during heating, as shown in Fig. 6a. Furthermore, the sample $\mathbf{1O}_{(2Y)}$ showed a different feature of the DTA curve, as shown in Fig. 6b, in which no heat anomaly appeared during cooling, but the endothermic peak which

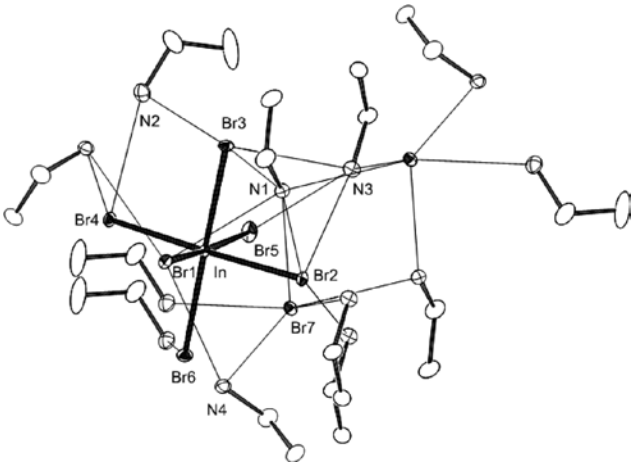

Fig. 2: Hydrogen bond scheme around the bromoindate and bromide anion in $\mathbf{1N}_{LTP}$.

Table 4: Short contact distances (pm) in $\mathbf{1N}_{LTP}$ which are shorter than the sum of the Van der Waals radii + 20 pm.[a]

	d(N···Br)		d(N···Br)
N1–H···Br1	354.7(4)	N3–H···Br3	359.0(4)
N4–H···Br1	342.4(4)	N2–H···Br4	339.9(4)
$N4^{\#1}$–H···Br1	344.9(4)	$N4^{\#2}$–H···Br4	354.9(4)
N1–H···Br2	344.2(4)	$N3^{\#3}$–H···Br5	344.8(4)
N3–H···Br2	343.0(4)	N3–H···Br5	355.9(4)
N1–H···Br3	337.6(3)	$N2^{\#4}$–H···Br6	344.7(4)
N2–H···Br3	355.9(4)		

[a]Symmetry operations: $^{\#1}$ 3/2 – *x*, 1/2 – *y*, 1/2 – *z*; $^{\#2}$ 3/2 – *x*, 1/2 + *y*, 1/2 – *z*; $^{\#3}$ 1 – *x*, 1 – *y*, 1 – *z*; $^{\#4}$ 1/2 – *x*, 1/2 + *y*, 1/2 – *z*.

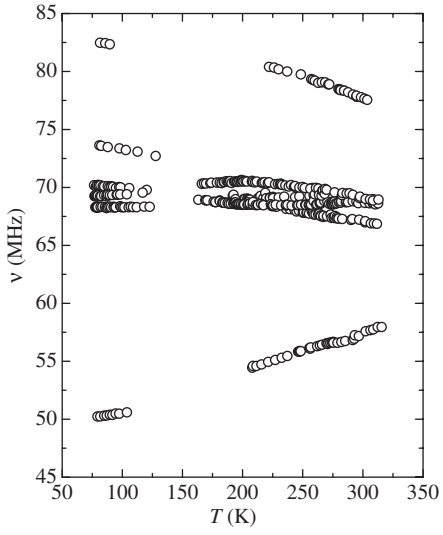

Fig. 3: Temperature dependence of ^{81}Br NQR frequencies of the newly prepared sample **1N**.

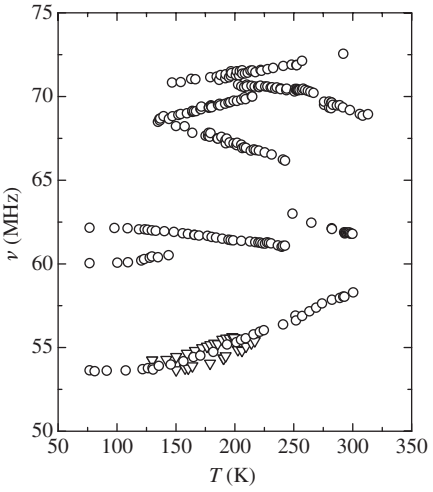

Fig. 4: Temperature dependence of ^{81}Br NQR frequencies of extra NQR lines of $\mathbf{1O}_{(10Y)}$ and $\mathbf{1O}_{(2Y)}$. The lowest-frequency line showed frequency changes on every measurment.

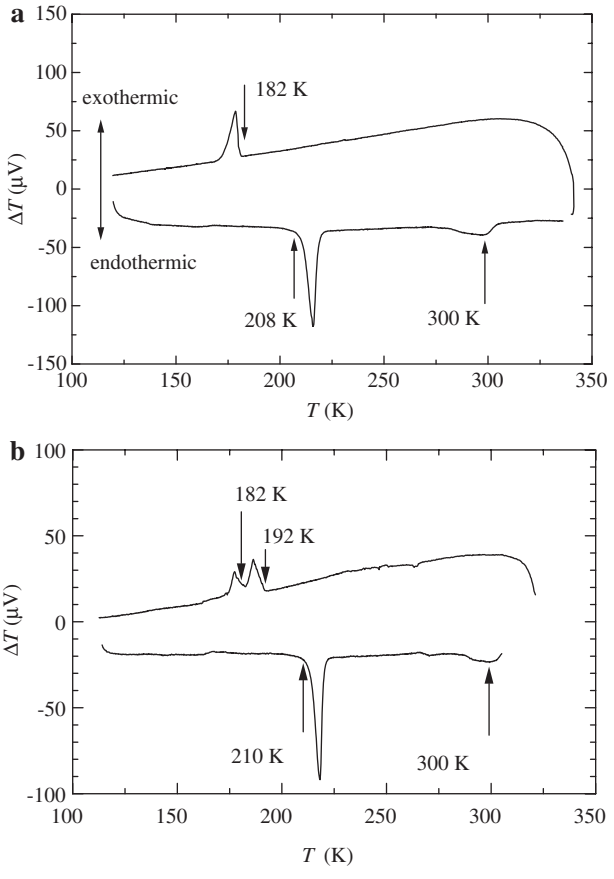

Fig. 5: (a) DTA curve of **1N**. The upper curve indicates the cooling run and the lower curve the heating run. (b) DTA curve of $\mathbf{1O}_{(6M)}$. The upper curve indicates the cooling run and the lower curve the heating run.

was observed at around 320 K in a first heating cycle did appear. Interestingly, the endothermic peak diminished in size on the successive second heating run, though no

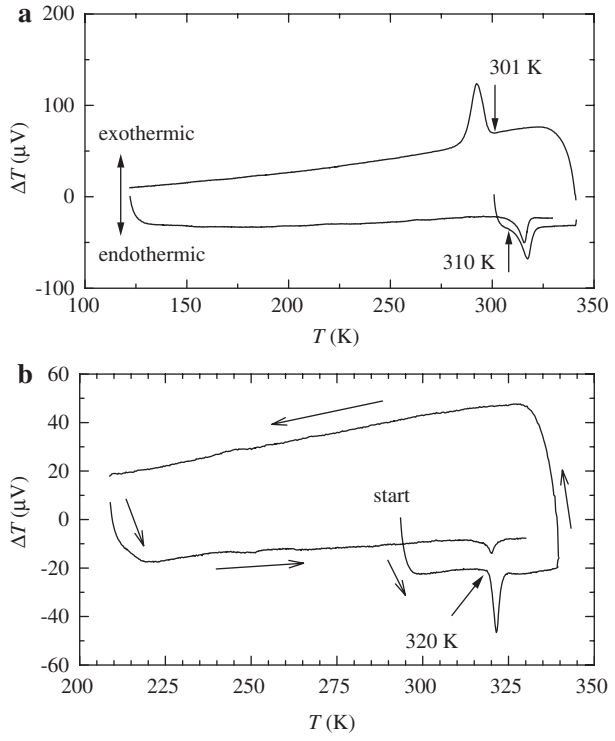

Fig. 6: (a) DTA curve of old sample $\mathbf{1O_{(10Y)}}$. The upper curve is the cooling run and the lower curve the heating run. (b) DTA curve of the old sample $\mathbf{1O_{(2Y)}}$. The upper curve is the cooling run and the lower curve the heating run.

difference in the peak size could be observed in the case of $\mathbf{1O_{(10Y)}}$. The NQR and DTA results indicate the occurrence of a structural change from **1N** to $\mathbf{1O_{(10Y)}}$. To confirm this, the C, H, and N elemental analyses were applied to the specimens of $\mathbf{1O_{(10Y)}}$ and $\mathbf{1O_{(2Y)}}$: found C 9.98, H 3.41, N 5.80 for $\mathbf{1O_{(10Y)}}$; found C 10.41, H 3.52, N 6.12 for $\mathbf{1O_{(2Y)}}$. When these values are compared with the calculated ones: C 9.83, H 3.30, N 5.73 for $[C_2H_5NH_3]_3InBr_6$ and C 11.19, H 3.75, N 6.52 for $[C_2H_5NH_3]_4InBr_7$ (**1N**), the values for $\mathbf{1O_{(10Y)}}$ coincide closely with the former values and those for $\mathbf{1O_{(2Y)}}$ are situated at an intermediate between the former and the latter. Therefore, it is deduced that a decomposition reaction, $[C_2H_5NH_3]_4InBr_7$ (**1N**) $\rightarrow [C_2H_5NH_3]_3InBr_6 + [C_2H_5NH_3]Br$, proceeds gradually at ambient temperature. The DTA curves in Fig. 6a therefore correspond to those of $[C_2H_5NH_3]_3InBr_6$. Furthermore, the DTA curves in Figs. 5b and 6b may be attributable to those of the mixtures in the transformation process from $[C_2H_5NH_3]_4InBr_7$ to $[C_2H_5NH_3]_3InBr_6$.

2.3 Crystal structure determination of tris(guanidinium) hexabromoindate(III) $[C(NH_2)_3]_3InBr_6$ (2)

The crystal structure of **2** has been determined from data collected at 100 K. The projection of the unit cell of **2** down the *a* axis is shown in Fig. 7. The asymmetric unit consists of three octahedral $[InBr_6]^{3-}$ ions and six $C(NH_2)_3^+$ ions. The respective ions have the local symmetry shown in the brackets as follows: $[(In1)Br_6]^{3-}$ [*E*], $[(In2)Br_6]^{3-}$ [C_{2v}], $[(In3)Br_6]^{3-}$ [D_{2h}], and all $C(NH_2)_3^+$ [*E*]. Wyckoff positions are 8*f*, 4*e*, 4*a*, and 8*f* for In1, In2, In3, and all Br atoms, respectively. Therefore, 12 nonequivalent Br atoms exist in **2**. The In–Br bond lengths are in the range of 261.86(2) to 272.39(5) pm (Table 2), and the bond angles ∠Br–In–Br (*cis*) range from 85.38(1) to 93.24(1)° (Table 3). These values are comparable with the corresponding values of 262.27(4) to 273.98(4) pm and 86.60(1) to 93.95(2)° in **1**. The hydrogen bond network built up between anions and cations can be seen in Fig. 8.

2.4 NQR measurements of $[C(NH_2)_3]_3InBr_6$ (2)

The temperature dependence of ^{81}Br NQR frequencies of **2** observed between 77 K and around 300 K is shown

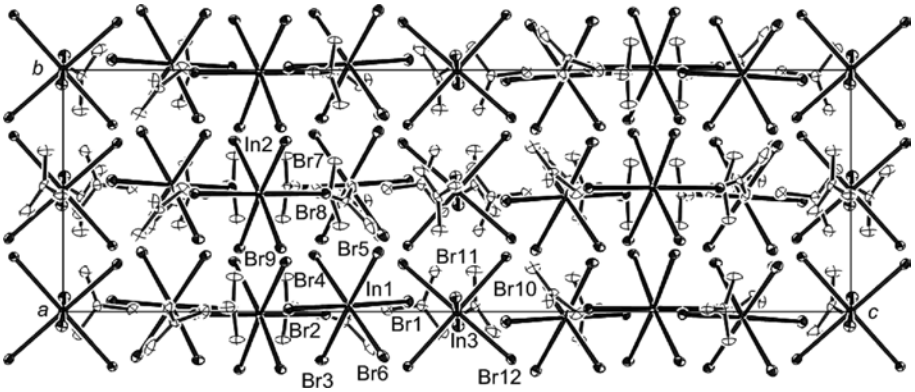

Fig. 7: Projection of the crystal structure of **2** at 100 K down the crystallographic *a* axis.

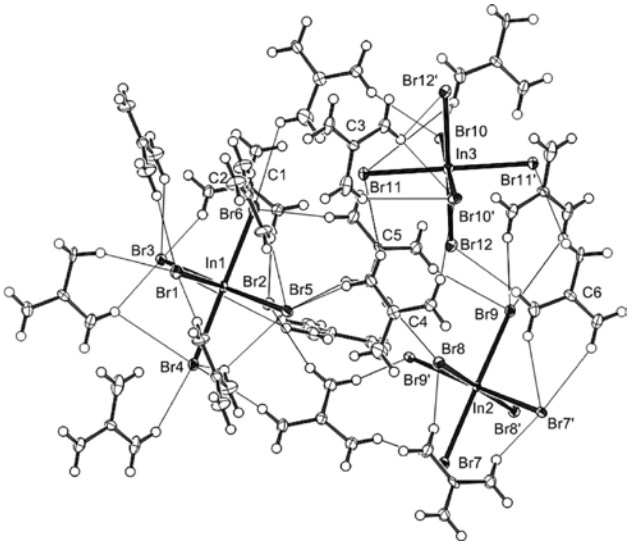

Fig. 8: Hydrogen bond scheme around the bromoindate anion in **2**.

in Fig. 9. According to the crystal structure, 12 ^{81}Br NQR lines with the same intensity are expected, but only 10 ^{81}Br NQR lines could be observed, with the remaining 2 NQR lines missing. The overlapping between a number of ^{81}Br and ^{79}Br NQR lines makes it difficult to completely resolve the respective lines. However, the monotonic temperature dependence suggests no occurrence of a phase transition in the measured temperature range. Interestingly, some NQR lines show positive temperature coefficients, whereas the others show negative but quite small temperature coefficients. This indicates that all the Br atoms are involved more or less in hydrogen bonds, as found in the crystal structure, which may be weakened according to the excitation of cation motions with increasing temperatures.

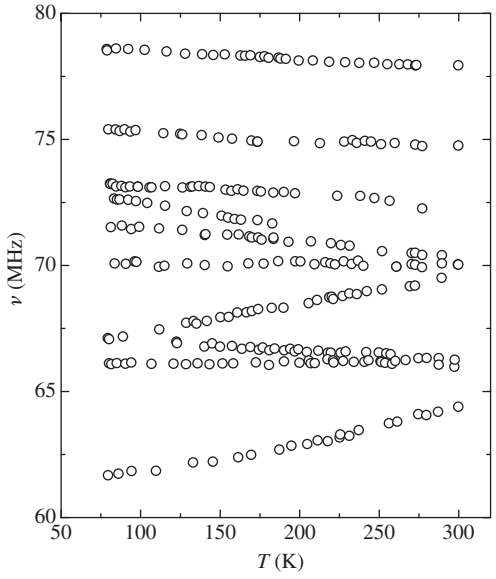

Fig. 9: Temperature dependence of ^{81}Br NQR frequencies of **2**.

2.5 Crystal structure determination of 2,2-dimethyl-1,3-propanediammonium pentabromoindate (III) of $[H_3NCH_2C(CH_3)_2CH_2NH_3]InBr_5$ (3)

The crystal structure of **3** has been determined from diffraction data collected at 100 K. The projection of the unit cell of **3** down the *b* axis is shown in Fig. 10. The asymmetric unit consists of one tetrahedral $[InBr_4]^-$, one double-octahedral $[In_2Br_{11}]^{5-}$, and three $H_3NCH_2C(CH_3)_2CH_2NH_3^{2+}$ ions. The $[InBr_4]$ tetrahedron of the central In3 atom is severely distorted with In3–Br bond lengths ranging from 250.2(10) to 256.34(10) pm and ∠Br–In3–Br bond angles from 100.20(3) to 132.00(4)°, as listed in Tables 2 and 3, respectively. The $[In_2Br_{11}]^{5-}$ ion is a corner-sharing dimer of

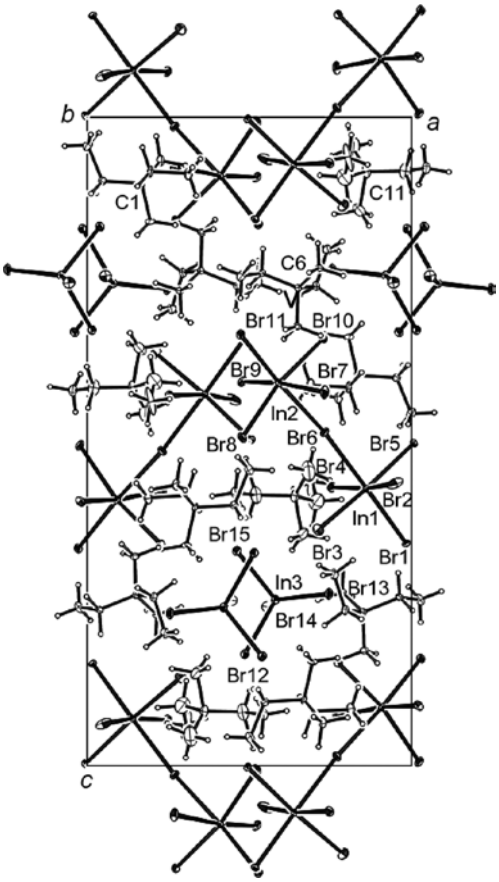

Fig. 10: Projection of the crystal structure of **3** at 100 K down the crystallographic *b* axis. Cations with the center cabon atom C11 are disordered.

two [$InBr_6$] octahedra with the central In1 and In2 atoms connected through the Br6 atom. The bridging bonds In1–Br6 and In2–Br6, being 297.82(9) and 301.66(9) pm, respectively, are considerably longer compared to the terminal bonds ranging from 262.01(9) to 270.36(9) pm in the In1 octahedron and from 260.05(10) to 267.26(10) pm in the In2 octahedron. There are thus 15 nonequivalent Br atoms in the crystal structure. One of three 2,2-dimethyl-1,3-propanediammonium cations, including C11 as a central atom of the propane skeleton, is disordered, with a CH_3 and a CH_2NH_3 groups placed between two positions leaving the remaining CCH_2NH_3 groups ordered. The hydrogen bond network of the ions is shown in Fig. 11.

2.6 NQR and DTA measurements of $[H_3NCH_2C(CH_3)_2CH_2NH_3]InBr_5$(3)

The temperature dependence of the ^{81}Br NQR frequencies in **3** observed up to around 310 K is shown in Fig. 12. All NQR lines except for the line situated at 70 MHz were observed as doublets with the intensity ratio of about 1 : 2 at 77 K. The spectra of representative doublet lines at 59, 62, and 80 MHz are shown and compared with those of two lines well separated in frequency in Fig. 13. The frequency difference between two lines in each doublet is less than 200 kHz, which is nearly equal to the quench frequency of 180 kHz in the super-regenerative oscillator-detector used for measurements. However, the spectra of the doublets are apparently different in their appearance from the side bands, as shown in Fig. 13. The stronger components of these doublets take the higher- or lower-frequency

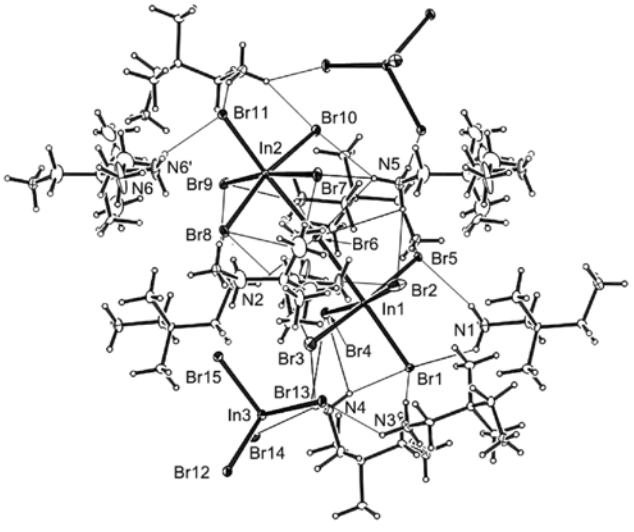

Fig. 11: Hydrogen bond scheme around $[In_2Br_{11}]^{5-}$ and $[InBr_4]^-$ ions.

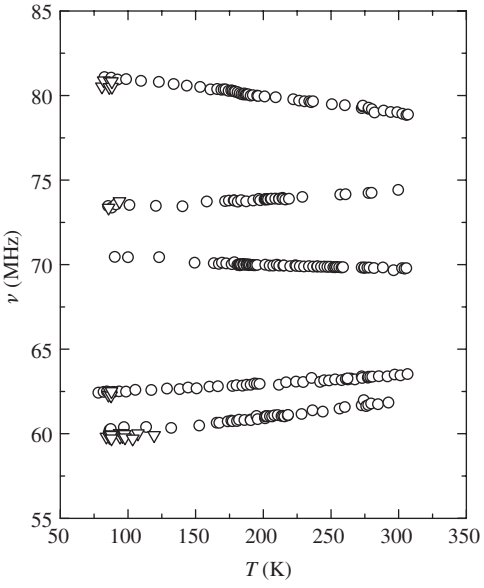

Fig. 12: Temperature dependence of ^{81}Br NQR frequencies of **3**.

positions independently of each other. With increasing temperature the weaker components of respective doublets are weakened rapidly in their intensities to become unobservable under the noises, whereas the stronger ones can be observed. As a result, five ^{81}Br NQR lines are observed in the searched range from 40 to 110 MHz, though the crystal structure requires 15 nonequivalent Br atoms. The resonance frequencies of the observed lines are almost comparable with those of the ^{81}Br NQR lines in **1** and **2**, indicating that these lines are attributable to the terminal Br atoms of the double-octahedral $[In_2Br_{11}]^{5-}$ ion, even though the number of lines is decreased to a half of those expected from the crystal structure at 100 K. On the other hand, the DTA measurements of **3** revealed the occurrence of phase transitions shown by an exothermic heat anomaly at 184 K accompanied by a small peak at 187 K on the cooling run and the endothermic one at 189 K while heating, as shown in Fig. 14. The hysteresis for the anomaly and the peak shape show the phase transition to be a first-order one. On the other hand, the ν versus T curves of ^{81}Br NQR lines show smooth changes in the vicinity of the phase transition points without showing any recognizable anomalies. This fact may be understandable if the phase transition is induced by the change in cation dynamics and is followed by almost no substantial changes in the anion structure. The crystal structure at 100 K in the LTP has revealed that one of the three cations is partially disordered. Furthermore, it is noticed that the disordered NH_3 groups of N6 and N6′ are hydrogen-bonded to 5 atoms of the 10 terminal Br atoms (Br2, Br3, Br7, Br8, and Br11), as plotted in Fig. 15. When the disorder fluctuates with the electric field

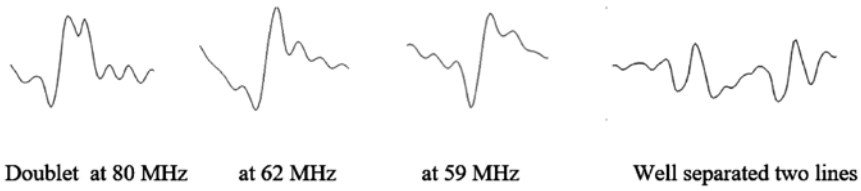

Fig. 13: NQR spetra collected at around 77 K. These spectra are obtained after numerical integration of raw recorded spectra.

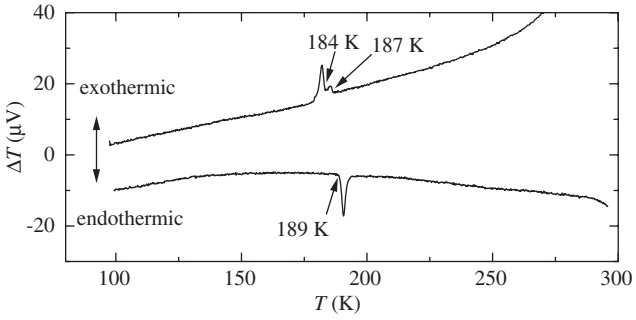

Fig. 14: DTA curve of **3**. The upper curve is the cooling run and the lower curve is the heating run.

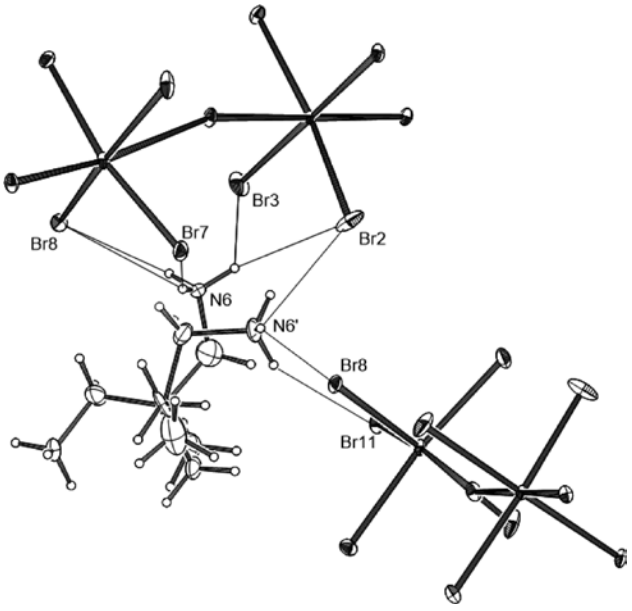

Fig. 15: Hydrogen bond scheme around disordered N6 and N6′ atoms at 100 K.

around these Br atoms, it is plausible that the intensities of ^{81}Br NQR lines are weakened to become unobservable and only half of the lines of the 10 terminal Br atoms are thus observed. Then, the weaker components of the doublets observed around 77 K should be attributable to the Br atoms being hydrogen bonded to the disordered cation, which become quickly unobservable with increasing fluctuation. On the other hand, the absence of an indication on the temperature dependence curves of ^{81}Br NQR lines at the phase transition can be realized, if the phase transition is characterized by the conversion between a static and a dynamic disorder structure of the disordered cation. The disordered cations fixed at one of two sites in the LTP can thus exchange their positions between two possible sites dynamically in the room-temperature phase (RTP). Furthermore, the dynamic disordering seems to be frozen via two steps to the static disordered state, as two exothermic peaks follow the phase transition from RTP to LTP. As a result, the ^{81}Br NQR lines of five terminal Br atoms in the $[In_2Br_{11}]^{5-}$ ions which take part in hydrogen bonding with the ordered cation have been observed throughout the measured temperature range, whereas those of the remaining five terminal Br atoms which take part in the hydrogen bonding with the disordered cation have been observed partially only in the vicinity of 77 K. The ^{81}Br NQR line of the bridging Br6 atom with the angle of 164.23(4)° in the $[In_2Br_{11}]^{5-}$ ion and the ^{81}Br NQR lines of the $[InBr_4]^-$ ion have not been observed in this experiment, as they appear beyond the frequency range we searched up to 110 MHz. Higher frequencies are expected according to the MO calculations as described in the next section. The NQR frequencies of the bridging halogen atoms having a bridging angle of nearly 180° are known to be higher than those of terminal halogen atoms [5].

2.7 MO calculations

MO calculations were applied to the respective anions of **1** and **3** to estimate the ^{81}Br NQR data (frequency and asymmetry parameter) and the bond angles defined as the angles between the *z* principal axes of EFG tensors. In the calculations, the crystal field effect was not considered. Details of calculation are described elsewhere [5]. The ^{81}Br NQR frequencies (MHz) and the asymmetry parameters calculated are as follows: *For the $[InBr_6]^{3-}$ ion in* ***1***, (Br1: 92.02 MHz, 0.00), (Br2: 91.37 MHz, 0.00), (Br3: 87.23 MHz, 0.00), (Br4: 93.31 MHz, 0.00), (Br5: 92.72 MHz, 0.00), and (Br6: 92.40 MHz, 0.00) with the averaged frequency of 91.51 MHz; *for the $[InBr_4]^-$ ion in* ***3***, (Br12: 145.83 MHz, 0.01), (Br13: 165.84 MHz, 0.00), (Br14: 164.05 MHz, 0.00),

and (Br15: 145.52 MHz, 0.01) with the averaged frequency of 155.24 MHz ; *for the $[In_2Br_{11}]^{5-}$ ion in* ***3***, (Br1: 76.59 MHz, 0.00), (Br2: 98.09 MHz, 0.01), (Br3: 94.58 MHz, 0.01), (Br4: 93.56 MHz, 0.01), (Br5: 91.06 MHz, 0.01), (Br6: 163.73 MHz, 0.12), (Br7: 112.38 MHz, 0.02), (Br8: 106.54 MHz, 0.02), (Br9: 97.62 MHz, 0.02), (Br10: 99.16 MHz, 0.03), and (Br11: 80.73 MHz, 0.00) with the averaged frequency of 95.03 MHz except for bridging Br6. The average values of the calculated frequencies are approximately 1.32 and 1.37 times higher than the observed ones for the $[InBr_6]^{3-}$ and $[In_2Br_{11}]^{5-}$ ions, respectively. The contribution of the crystal field effects to the EFGs around the relevant Br atoms is thus considered to be roughly 25%, which may reduce the ^{81}Br NQR frequencies. The angles between the *z* principal axes of the EFG tensors are listed in Table 3 and compared with the bond angles from the X-ray structures. For the $[InBr_6]^{3-}$ ion of **1**, both angles are in good accordance with deviations within 1°. For the $[InBr_4]^-$ and $[In_2Br_{11}]^{5-}$ ions of **3**, the angles are also in good accordance, but with several exceptions where the maximum difference reaches up to around 10°. Especially large discrepancies are seen between the angles related to the terminal Br14 atom of $[InBr_4]^-$ and the bridging Br6 atom of $[In_2Br_{11}]^{5-}$. These discrepancies for the $[InBr_4]^-$ and $[In_2Br_{11}]^{5-}$ ions of **3** can be attributed to the packing of the molecules which incorporates two kinds of complex anions with different coordination structures. The packing with maximum crystallization energy may cause deviations of the bond directions from the principal axes.

3 Conclusions

The crystal structures of the bromoindate(III) complexes with organic ammonium cations may be characterized by a variety of anions. Thus, it was found that one octahedral $[InBr_6]^{3-}$ ion and one Br^- ion exist in $[C_2H_5NH_3]_4InBr_7$ (**1**), three kinds of octahedral $[InBr_6]^{3-}$ ions in $[C(NH_2)_3]_3InBr_6$ (**2**), and one double-octahedral $[In_2Br_{11}]^{5-}$ ion and one tetrahedral $[InBr_4]^-$ ion in $[H_3NCH_2C(CH_3)_2CH_2NH_3]InBr_5$ (**3**). It has been found previously that two kinds of isolated octahedral $[InBr_6]^{3-}$ ions exist in $[(CH_3)_2NH_2]_3InBr_6$ and a square pyramidal $[InBr_5]^{2-}$ ion in $[4\text{-}ClC_5H_4NH]_2InBr_5$. The above results indicate that In(III) prefers to take the octahedral coordination of $[InBr_6]$ in all compounds of different compositions. Lower coordination numbers as in the $[InBr_5]$ complexes are rare.

The present results also show that the N–H···Br–In hydrogen bonds between the cations and anions develop well to form a network in the crystal structures, which allows us to categorize these crystal structures as hydrogen bonded as well the ionic crystal structures. Reflecting the hydrogen bonds, the ^{81}Br NQR frequencies are widely spread in frequency and some of the resonance lines have unusual positive temperature coefficients, which manifests the polarizations of In–Br bonds due to the hydrogen bonds and the dynamic motions of cations connected to the hydrogen bonds. The occurrence of phase transitions in $[C_2H_5NH_3]_4InBr_7$ (**1**) and $[H_3NCH_2C(CH_3)_2CH_2NH_3]InBr_5$ (**3**) demonstrates that the stability of the present type of crystals is dependent on a subtle balance between electrostatic force and hydrogen bonding.

The MO calculations have given higher values than the measured ones for the ^{81}Br NQR frequencies, as expected considering the structural details. Accurate bond angles have been estimated with several exceptions. The present calculations together with previous ones [5] show the usefulness of the MO calculations for estimating the crystalline field effects and the crystal packing effects of the molecules in the present type of crystals.

4 Experimental section

4.1 Sample preparation

A stock solution of $InBr_3$ was prepared by dissolving In metal (> 99.9%, Sigma-Aldrich) in 48% aqueous HBr solution (special grade, Wako) and by adding water resulting in 20% HBr content for the syntheses of all compounds. The crystals of **1** were prepared by adding 0.2 mol of $[C_2H_5NH_3]Br$ (special grade, Wako) into $InBr_3$ stock solution containing 0.05 mol of $InBr_3$. Colorless needle-like crystals (**1N**) appeared after the removal of water from the solution by P_2O_5 in a desiccator at room temperature. On keeping the crystals in the mother liquor, **1N** turned gradually into massive crystals. A needle crystal of **1N** for the X-ray measurement was picked from the freshly prepared solution. The crystals of **2** were obtained during an attempt of preparation of $[C(NH_2)_3]InBr_4$ by adding 0.1 mol of $[C(NH_2)_3]_2CO_3$ (first grade, Wako) and 0.3 mol of HBr as 48% aqueous solution into $InBr_3$ stock solution containing 0.2 mol of $InBr_3$. On removing the water from the solution by P_2O_5 in a desiccator, colorless square prismatic crystals appeared. A suitable crystal was selected from them for the X-ray measurement. The crystals of **3** were obtained by adding 0.1 mol of 2,2-dimethyl-1,3-proanediamine and 0.3 mol of HBr as 48% aqueous HBr solution into $InBr_3$ stock solution containing 0.1 mol of $InBr_3$. Concentrating the solution by heating, feather-like crystals appeared initially, which turned into colorless tabular

crystals after dissolving by the addition of water and removing water by P_2O_5 in a desiccator. A tabular crystal was picked for the X-ray measurement. – Elemental analyses for **1N**: calcd. C 11.19, H 3.75, N 6.52; found C 10.80, H 3.65, N 6.30; for **2**: calcd. C 4.65, H 2.34, N 16.27; found C 4.59, H 2.30, N 15.84; for **3**: calcd. C 9.70, H 2.60, N 4.52; found C 9.77, H 2.56, N 4.52.

4.2 NQR and DTA measurements

The ^{81}Br and ^{79}Br NQR spectra were recorded by a home-made super-regenerative type spectrometer at temperatures above 77 K. The resonance frequencies were determined by a counting method. The accuracy of the frequency measurements is estimated to be within ±0.05 MHz. DTA was measured by a home-made apparatus at temperatures above 100 K.

4.3 Crystal structure determination

All measurements were made on a Bruker D8 Venture PHOTON area detector (MoK_α radiation, λ = 71.073 pm). Data were collected at 100 K and processed using Olex2 1.2 [6, 7]. The structures were solved by Direct Methods [8, 9] and expanded using Fourier techniques. All calculations were performed using the Olex2 1.2 crystallographic software package except for refinements which were performed using Shelxl [10–12]. Positional and displacement parameters and other experimental details can be obtained from The Cambridge Crystallographic Data Centre via www.ccdc.cam.ac.uk/data_requetst/cif (CCDC 1431879 for **1N**, 1431880 for **2**, and 1431881 for **3**).

4.4 MO calculation

The detailed description of the MO calculation on PM3 basis using Gamess (Windows version 2013), a quantum chemistry package [13], was reported elsewhere [5]. The population analysis was done for 4*p* orbitals of Br atoms in the $[InBr_6]^{3-}$ ion in **1**, and the $[In_2Br_{11}]^{5-}$ and $[InBr_4]^-$ ions in **3**. The structural information of the ions was taken from the crystal structures determined. Facio 19.1.4 [14, 15] and Mercury 3.6 [16, 17] were used for the support of the MO calculations.

References

[1] A. J. Carty, D. G. Tuck, *Prog. Inorg. Chem*. **1975**, *19*, 243.
[2] H. Ishihara, S. Dou, T. M. Gesing, H. Paulus, H. Fuess, A. Weiss, *J. Mol. Struct*. **1998**, *471*, 175.
[3] M. A. Khan, D. G. Tuck, *Acta Crystallogr*. **1981**, *B37*, 683.
[4] H.-U. Schlimper, M. L. Ziegler, *Z. Naturforsch*. **1972**, *27b*, 377.
[5] T. M. Gesing, E. Lork, H. Terao, H. Ishihara, *Z. Naturforsch*. **2016**, *71b*, 241.
[6] Olex2 (version 1.2): A Complete Structure Solution, Refinement and Analysis Program, Durham University, Durham (U.K.) **2009**.
[7] O. V. Dolomanov, L. J. Bourhis, R. J. Gildea, J. A. K. Howard, H. Puschmann, *J. Appl. Crystallogr*. **2009**, *42*, 339.
[8] G. M. Sheldrick, Shelxs-97, Program for the Solution of Crystal Structures, University of Göttingen, Göttingen (Germany) **1997**.
[9] G. M. Sheldrick, *Acta Crystallogr.* **1990**, *A46*, 467.
[10] G. M. Sheldrick, Shelxl-97, Program for the Refinement of Crystal Structures, University of Göttingen, Göttingen (Germany) **1997**.
[11] G. M. Sheldrick, *Acta Crystallogr.* **2008**, *A64*, 112.
[12] G. M. Sheldrick, *Acta Crystallogr*. **2015**, *C71*, 3.
[13] M. W. Schmidt, K. K. Baldridge, J. A. Boatz, S. T. Elbert, M. S. Gordon, J. H. Jensen, S. Koseki, N. Matsunaga, K. A. Nguyen, S. J. Su, T. L. Windus, M. Dupuis, J. A. Montgomery, *J. Comput. Chem*. **1993**, *14*, 1347.
[14] M. Suenaga, *J. Comput. Chem. Jpn.* **2005**, *4*, 25.
[15] M. Suenaga, *J. Comput. Chem. Jpn.* **2008**, *7*, 33.
[16] Mercury (version 3.6 for Windows), Crystal Structure Visualisation, Exploration and Analysis Made Easy, Cambridge Crystallographic Data Centre (CCDC) **2015**.
[17] C. F. Macrae, I. J. Bruno, J. A. Chisholm, P. R. Edgington, P. McCabe, E. Pidcock, L. Rodriguez-Monge, R. Taylor, J. van de Streek, P. A. Wood, *J. Appl. Crystallogr.* **2008**, *41*, 466.